International Journal of Heat and Mass Transfer 228 (2024) 125597

Contents lists available at ScienceDirect

International Journal of Heat and Mass Transfer

journal homepage: www.elsevier.com/locate/ijhmt

Experimental investigations of effects of nanoparticle size on force convective heat transfer characteristics of Al_2O_3 - MWCNT hybrid nanofluids in transitional flow regime

Ibrahim Umar Ibrahim [a,b], Mohsen Sharifpur [a,c,d,*], Josua P. Meyer [a,e], S M Sohel Murshed [f,*]

[a] Department of Mechanical and Aeronautical Engineering, University of Pretoria, Pretoria 0002, South Africa
[b] Department of Mechanical Engineering, Ahmadu Bello University Zaria, Kaduna State, Nigeria
[c] School of Mechanical, Industrial and Aeronautical Engineering, University of the Witwatersrand, Private Bag 3, Wits 2050, South Africa
[d] Department of Medical Research, China Medical University Hospital, China Medical University, Taichung, Taiwan
[e] Department of Mechanical and Mechatronic Engineering, Stellenbosch University, Stellenbosch, South Africa
[f] IDMEC, Department of Mechanical Engineering, Instituto Superior Tecnico, University of Lisbon, 1049-001 Lisbon, Portugal

ARTICLE INFO

Keywords:
Transition flow
Hybrid nanofluid
Nusselt number
Heat transfer coefficients
Coefficient of thermal performance
Particle size

ABSTRACT

This study reports an experimental investigation of nanoparticle sizes effects on the heat transfer characteristics of hybrid nanofluids along the transitional flow regime. Four different particle sizes were used to prepare hybrid nanofluids of Al_2O_3 and MWCNT (i.e., 5 nm and 20 nm for Al_2O_3 and <7 nm and 30–50 nm for MWCNT nanoparticles). Three hybrid nanofluids with different particle combinations (i.e., Al_2O_3(5 nm) – MWCNT (<7 nm), Al_2O_3(20 nm) – MWCNT(<7 nm) and Al_2O_3(20 nm) – MWCNT (30–50 nm)) at a percentage weight composition (PWC) of 60:40 and 0.3 volume concentration were prepared. Results showed that particle sizes significantly affected the convective heat transfer characteristics of the nanofluids. Along the transition region, all three fluids were found to have different critical Reynold numbers 1152, 1172, and 1898 for Al_2O_3(20 nm) – MWCNT (<7 nm), Al_2O_3(5 nm) – MWCNT (<7 nm) and Al_2O_3(20 nm) – MWCNT (30–50) respectively. Al_2O_3(20 nm) – MWCNT (<7 nm) have shown better heat transfer performances. Its Nusselt number shows an enhancement of about 48.86 % along the transition region. And its coefficient of thermal performance (COP) was better than that of Al_2O_3(20 nm) – MWCNT (30–50 nm) and Al_2O_3(5 nm) – MWCNT (<7 nm) with 43.53 % and 21.89 %, respectively. While its friction factor and pressure drop were lower than that of Al_2O_3(5 nm) – MWCNT (<7 nm) nanofluid by 5.2 % and 12.78 %. It was concluded that for a 60:40 hybrid nanofluid of Al_2O_3 and MWCNT, particle sizes have influenced heat transfer characteristics and affected other flow characteristics along the transition regime.

1. Introduction

Recent advancements in science and technology have brought about the design of miniaturised thermal devices, which require optimum and efficient thermal management. Generally, the smaller the size, the greater the need for an efficient cooling system [1,2]. Meanwhile, miniaturised devices possess challenges in managing their thermal performance. Many researchers have been drawn to the thermal management of miniaturised devices to develop efficient and cost-effective heat removal systems. The fact that existing coolants (e.g., water, ethylene glycol (EG), propylene glycol (PG), automatic transmission fluid (ATF), oils, etc.) lack the necessary or adequate cooling capacity needed for the effective functioning of these new cooling technologies make it even more challenging [3,4]. Among other issues, the low thermal conductivity of these conventional fluids limited their capacity and ability to improve the thermal efficiency of these devices [5]. Therefore, there is a need to develop an improved cooling system and innovative coolants with higher thermal conductivity [6]. Several ways have been developed to enhance heat transfer between fluids and surfaces in contact with the fluid [7,8]. Current heat transfer fluids, such as water, oils, and ethylene glycol/water, have poor thermal properties compared to solids [7]. Therefore, the dispersion of nanoparticles into base fluids improves the thermal properties of these fluids [3].

Nanofluids were designated as new heat transfer fluids because they provide fascinating new prospects for increasing heat transfer

* Corresponding authors.
E-mail addresses: mohsen.sharifpur@up.ac.za (M. Sharifpur), smurshed@tecnico.ulisboa.pt (S.M.S. Murshed).

https://doi.org/10.1016/j.ijheatmasstransfer.2024.125597
Received 15 June 2023; Received in revised form 4 April 2024; Accepted 18 April 2024
Available online 11 May 2024

Nomenclature

A_S	surface area, m^2
C_{bf}	specific heat capacity of base, J/kg-K
C_{hnf}	specific heat capacity of hybrid, J/kg-K
c_p	specific heat capacity of particles, J/kg-K
D_i	internal tube diameter, m
D_O	outer tube diameter, m
$h(x)$	local heat transfer coefficient, W/m^2 -K
h_{avg}	average coefficient of heat transfer, W/m^2-K
I	current, A
J	colburn J factor.
k	thermal conductivity, W/m-K
k_{cu}	thermal conductivity of the copper, W/m-K
L	test section length, m
$\dot{m}$	mass flow rate, kg/s
Nu(x)	local Nusselt number.
Nu_{avg}	average Nusselt number.
P	the perimeter of the tube, m
Pr	Prandtl number.
$\dot{Q}_e$	electric energy supply rate, W
$\dot{q}$	heat flux, W/m^2
$\dot{Q}_f$	heat transfer rate, W
Re	Reynolds number.
Re_{cr}	critical Reynold number
T_a	ambient temperature, °C
T_i	inlet temperature, °C
$T_f(x)$	local mean fluid temperature, °C
T_b	bulk temperature, °C
$T_{si}(x)$	inside wall temperature, °C
$T_{so}(x)$	outside wall temperature, °C
v	voltage, V
x	distance from the tube inlet, m
R_m	resistance of the tube material

Greek Letters

ρ_{hnf}	density of the hybrid nanofluid, kg/m^3
ρ_{bf}	base fluid density, kg/m^3
ρ_p	density of particles, kg/m^3
μ	viscosity, kg/m. s
ν	kinematic viscosity, m^2/s
ρ	density, kg/m^3
φ	volume concentration

Subscripts

o	outlet/out
i	inlet/internal
f	fluid
s	surface
a	ambient/ atmospheric
avg	average
cr	critical
hnf	hybrid nanofluid
bf	base fluid.
P	particles
cu	copper
e	electrical
si	inside wall
so	outside wall
m	materials
b	bulk

Abbreviation

PWC	percentage weight compositions
COP	coefficient of thermal performance
HTC	heat transfer coefficient
HNF	hybrid nanofluid

performance [9–12]. Kole et al. [13] investigated graphene-based nanofluid thermal conductivity and viscosity. They noticed that adding graphene particles to the base fluid enhanced the heat conductivity of the base fluid by roughly 15 %. This demonstrates the importance of incorporating these nanoparticles with conventional heat transfer fluids. Many review works (e.g., [14]) and numerous investigations on the thermal conductivity of different types of nanofluids reaffirmed the importance of these fluids in the future [15–17]. Several research studies were conducted on the performance of nanofluids under forced convective heat transfer conditions, especially in laminar and turbulent regions, and they all indicated better enhancement with nanofluids than with conventional fluids [15–17]. Azari et al. [18] studied different nanofluids convective heat transfer performance under a laminar flow regime. The fluids evaluated were Al_2O_3, TiO_2, and SiO_2, with deionised water as the base fluid. The results show that adding these nanoparticles enhances base fluid heat transfer by an average of about 16 % and 8.2 % with nanoparticles of Al_2O_3 and TiO_2, respectively. Akhavan-Zanjani et al. [19] found out that the heat transfer coefficient of water was enhanced by about 14.2 % when 0.02 % by volume fraction of graphene nanoparticles were added. In a similar study, Nourafkan et al. [20] used cuprous oxide (Cu_2O)-water nanofluid to investigate the influence of dispersed nanoparticles. Results show an average enhancement of about 10 % in the forced convection. However, Nourafkan et al. [20] learned that there is a penalty in terms of friction factor, which has risen by about 16 %. They conclude that dispersed particles' stochastic mobility amplifies the convective heat transfer. Aghabozorg et al. [21], Ding et al. [22], and Sundar et al. [23] all reported that the nanofluid convective heat transfer coefficient increases with the increase in volume concentration. Some significant research findings were also reported with hybrid nanofluid. Especially on the convective heat transfer characteristics in the lamina and turbulent regimes. Megatif et al. [24] investigated the heat transfer characteristics of TiO_2–CNT hybrid nanofluids under a lamina regime. Two volume concentrations of 0.1 % and 0.2 % were evaluated. Results show a significant improvement in the heat transfer characteristics with 0.2 % volume concentration. Gupta et al. [25] also reported a 59.8 % enhancement of convective heat transfer coefficient with 0.5 % volume concentration of Ag-MWCT hybrid nanofluid along the lamina region. While the research work of Suresh et al. [26] shows an enhancement of about 14 % recorded at $Re = 1730$ with Al_2O_3-DI water nanofluids.

The transition region is one of the regions of interest because research shows there is a possibility of several advantages in this regime that are yet to be appropriately utilised. It will likely have an improved heat transfer along the region [27]. However, because of inadequate knowledge of flow characteristics along the region, heat exchangers are typically designed not to operate along this region [28]. Another reason was the high uncertainty and unreliability of the flow in the region. This makes predictions along this regime very unreliable and uncertain [28]. Although the transition regime has a short Reynold number range, research shows that its start and end can be affected by several factors, like inlet configurations, tube roughness, heat flux, etc. [29,30]. Most of the research works in this field use water, not nanofluids. But still, those findings help us better understand the regime characteristics. Notwithstanding, some researchers tried to investigate the heat transfer of nanofluids in this region, like Meyer et al. [31], Naik et al. [32], Chougule and Sahu [33], and Osman et al. [34].

A research investigation by Meyer et al. [31] using Multiwalled carbon nanotube nanofluid revealed that there is a better improvement

in heat transfer (Nu) along the transition region as compared to the other flow regimes (i.e., Laminar and turbulent). Naik et al. [32] also reported similar findings. In this research, they use helical inserts, and results show that using a 0.5 % volume concentration of CuO nanofluid, heat transfer was enhanced by about 28 % along the region. Chougule and Sahu [33] also observed a similar conclusion when investigating the heat transfer characteristics of Al_2O_3-water and MWCNT-water nanofluids along the transition regime. Four different concentrations (i.e., 0.15, 0.45, 0.60, and 1 % volume concentration) and three different inserts with varying twist ratios (i.e., 1.5, 2.5, and 3) were used. It was discovered that the heat transfer coefficient of nanofluids increased with increasing particle volume concentration. The most significant heat transfer enhancement was found with a 1 % volume concentration of MWCNT – Water nanofluid. But with inserts, the nanofluids friction factor increases to about 5.4 times that of the base fluid. This was also similar to the findings reported by Naik et al. [32], where the nanofluid friction factor rises by about 140 % with the addition of inserts.

The literature review above shows promising signs of enhanced heat transfer capabilities in the transition region with nanofluids. However, none of the research discussed dispersed nanoparticles influences on other regions characteristics. It was learned that the discussion focuses on nanofluid heat transfer enhancement and friction factor in the region. But there is a lot more to explore and investigate in the region. One crucial factor that needs attention is the regime boundary. The start and end of the transition region and the effects of particle sizes and their influence on the transition region have not yet been investigated experimentally, especially with a hybrid nanofluid.

Nanofluids have their own distinctive and peculiar characteristics that have a significant impact on their heat transfer behaviour. Factors like particle sizes, concentration, types of nanoparticles, etc., were very important in influencing their heat transfer characteristics [35]. The emergence of hybrid nanofluids (HNFs) set another new dimension of nanofluids research. These nanofluids (i.e., hybrid) have distinctive properties that differ from the single (mono) nanofluids. HNFs were prepared in a similar way to the single nanofluids. Still, because two different nanoparticles were hybridised in a specific weight percentage composition, their properties were different from the single nanofluids. In addition, the properties of HNFs also get affected when the percentage weight compositions (PWC) or particle sizes of each constituent's particles change [35].

Research findings show particle sizes are a critical factor affecting hybrid nanofluid characteristics. For example, Giwa et al. [35] explained that particle size influences the heat transfer performance of both single and hybrid nanofluids. However, this aspect was not thoroughly investigated in forced convection heat transfer. Therefore, an Al_2O_3 – MWCNT hybrid nanofluid was prepared in this research, but with a different particle size composition. Four different nanoparticle sizes of Al_2O_3 and MWCNT were used. For aluminum oxide (i.e., Al_2O_3), two sizes of 20 nm and 5 nm were used, while for MWCNT, particles with sizes 30–50 nm and 7 nm were used. Three HNF samples (Al_2O_3(20 nm) – MWCNT (30–50 nm), Al_2O_3(20 nm) – MWCNT(<7 nm) and Al_2O_3(5 nm) – MWCNT(<7 nm)) were prepared for this investigation. Only 0.3 volume concentration was considered in this experiment because Meyer et al. [31], Hameed et al. [36,37], and Osman et al. [34] research have investigated and discussed the effects of volume concentration on the lamina, turbulent and transition regions.

To the authors' knowledge, no research has been reported to study the effect of particle sizes under force convection heat transfer with the present HNFs, especially in the transition region. Although Anoop et al. [38] studied the effect of particle sizes in the developing flow, the work used only two particle sizes of Al_2O_3 of 45 nm and 150 nm, and the fluid prepared was a single nanofluid of Al_2O_3 with water as the base fluid. While research work by Hameed et al. [36,37] only investigated the heat transfer characteristics of Al_2O_3 (90 %) – MWCNT (10 %) nanofluid in the laminar and turbulent regime. It is important to note that Hameed et al. [36,37] research focuses on laminar and turbulent regimes, and no consideration was given to the effects of particle sizes, regime boundary conditions, or transition regimes. Findings from Hameed et al. [36,37] show that Al_2O_3 – MWCNT nanofluid has a better heat transfer enhancement when compared to compared to the Al_2O_3 – Cu hybrid nanofluid and 0.3 % volume concentration has the highest enhancement of about 22.11 % compared to the other concentrations examined.

Therefore, this research's primary aim and focus were on the transition regime and the effects of particle sizes on both heat transfer characteristics and transition boundary conditions (i.e., the start and end of the transition). This is very important and needs to be studied and understood before utilising their full potential in this regime.

2. Experimentation

2.1. Materials

Nanoparticles used in this study were bought from Nano Research Materials Inc. (USA), and they have the following physical data and properties (Table 1) and were used without any modifications.

2.2. Preparation of Al_2O_3 – MWCNT nanofluid

To investigate the influence of particle sizes on heat transfer characteristics of hybrid nanofluids in the transition region. Three hybrid nanofluids of Al_2O_3 – MWCNT were prepared using a two-step method with deionised water (DI water) as the base fluid. These nanofluids contain different combinations of Al_2O_3 and MWCNT particle sizes. Al_2O_3 particle sizes are 5 nm and 20 nm, while the MWCNT particles are particles with sizes less than <7 nm and particles between 30 and 50 nm. (i.e., Al_2O_3 (5 nm), Al_2O_3 (20 nm), MWCNT (<7 nm) and MWCNT (30–50 nm)). One volume concentration of 0.3 % was prepared with particle weight ratios of Al_2O_3 and MWCNT 60: 40, respectively. A 60:40 hybridisation ratio was chosen because results from the literature (e.g., [40]) showed significant improvement in thermal conductivity at this ratio. While a volume concentration of 0.3 % was chosen because a previous study [37] confirmed that this concentration resulted in better results than other volume concentrations. The fluids combination prepared are Al_2O_3 (5 nm) _ MWCNT (<7 nm), Al_2O_3 (20 nm) _ MWCNT (<7 nm), and Al_2O_3 (20 nm) _ MWCNT (30–50 nm).

Nanoparticles were weighed at a particle weight ratio of 60:40 (Al_2O_3 (60 %) and MWCNT (40 %)) and dispersed respectively into DI water. To improve the stability of the fluid, 0.5 wt.% of SDBS surfactant was used. The mixture was then put to magnetic stirring for 30 min and then sonicated for 1 hour at an amplitude of 90 using an Ultra-sonicator, which breaks the particle's agglomerations and properly disperses the nanoparticles in the base fluid. This approach was also used by Anoop et al. [38] and Nadooshan et al. [41], and the fluids were monitored for ten days without any sedimentation or agglomeration of the particles. This shows that the fluids have excellent stability, this is agreed with Krishnan et al. [40], who prepared and analysed the properties and stability of this hybrid nanofluid with different particle sizes using the same sonication and stirring parameters. Properties were characterised, including viscosity, thermal conductivity, electric conductivity, and pH. Fig. 1a presents the nanofluids immediately after preparations and after

Table 1
Summary of particles' physical properties.

Nanoparticles	Particle sizes [nm]	Purity	Specific heat [J/kg K]	Thermal conductivity [W/mK]
Al_{2O3}	20 and 5	99 %	880	37
MWCNT	<7 and 30–50	>95 %	711	3000

Source: Material Data sheets from Nano Research Materials Inc. (USA), (US4314) and Li et al. [39].

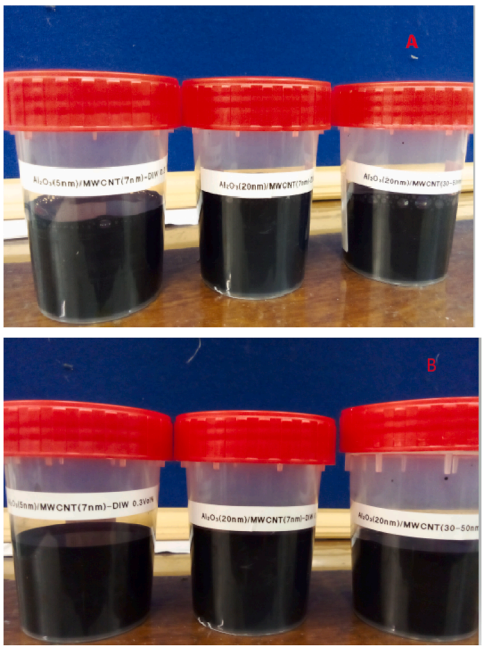

Fig. 1. Nanofluids preparations.

ten days in Fig. 1b.

Fig. 2. Shows the TEM images of the three nanofluids nanofluid prepared.

2.3. Thermophysical properties of the hybrid nanofluid

Fig. 3a shows the thermal conductivity of the hybrid nanofluids measured using a KD2 Pro-thermal conductivity meter at different temperatures between 10 °C and 30 °C. Results were compared with the Pak and Cho [42] correlation given by Eq. (1), and the correlation deviates from the measured result by less than 3 %. This is similar to the finding of Sharma et al. [43].

$$k_{nf} = k_w(1 + 7.47\varphi) \tag{1}$$

Fig. 3b. shows the viscosity of the hybrid nanofluids measured using Sv–10 Vibro Viscometer (A&D, Japan), which has an uncertainty of less than 5 % when operating at full capacity. The viscosity is compared to the water viscosity predicted by the popular classical model of Bachelor (available in [44]) and with the regression Eq. (2), as shown in Fig. 3b. The comparison was found by the method used by Sharma et al. [43] and Osman et al. [34].

$$\mu_{nf} = \mu_w\left(1 + 2.5\varphi + 6.2\varphi^2\right) \tag{2}$$

Fig. 4 demonstrates the pH and electrical conductivity data for the hybrid nanofluids. It can be seen that Al_2O_3 (5) – MWCNT(<7) has the highest pH value, while Al_2O_3 (20) – MWCNT(30–50), has the lowest pH value. Results also show that nanofluid's pH decreased with the increasing temperature, which is in accordance with the findings of Giwa et al. [35], Ibrahim et al. [45], and Krishnan et al. [40].

Electrical conductivity was measured using a CON 700 conductivity meter. The result shows that hybrid nanofluid electrical conductivity increases with the rise in temperature (Fig. 4b), which is similar to the finding of Giwa et al. [35]. Krishnan et al. [40] explained that the differences in electrical conductivity because of particle sizes in the hybrid nanofluid were caused by particle charge density, which is reduced with an increase in particle sizes.

The density of the hybrid nanoparticles of Al_2O_3 – MWCNT was calculated using Eq. (3) obtained from the literature [46], and it was found to be 3222 g/m^3, while the heat capacity (specific) of the hybrid

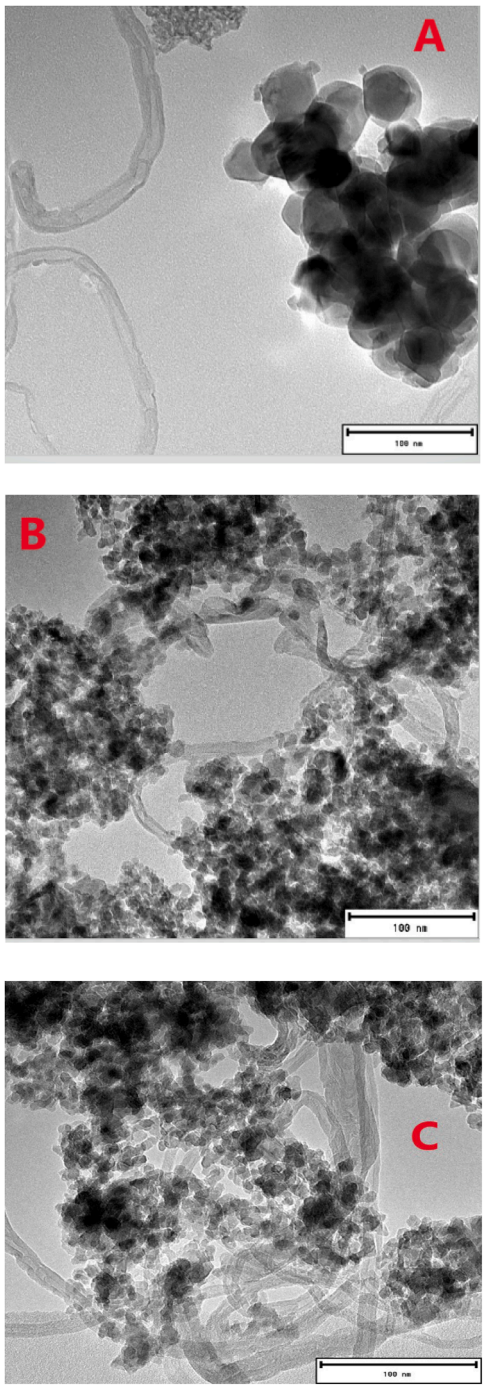

Fig. 2. TEM image of the hybrid nanofluid morphology.

nanoparticles was determined from the similar correlation given by Eq. (3) [45,46]

$$\rho_{(Al_2O_3-MWCNT)} = \frac{\left(\rho_{Al_2O_3}PWC_{Al_2O_3}\right) + \left(\rho_{MWCNT}PWC_{MWCNT}\right)}{\left(PWC_{Al_2O_3} + PWC_{MWCNT}\right)} \tag{3}$$

$$c_{(Al_2O_3-MWCNT)} = \frac{\left(c_{(Al_2O_3)}PWC_{Al_2O_3}\right) + \left(c_{MWCNT}PWC_{MWCNT}\right)}{PWC_{Al_2O_3} + PWC_{MWCNT}} \tag{4}$$

From the above equations, PWC is the percentage weight concentration of the nanoparticles in the hybrid mixture, where Al_2O_3 is 60 % and MWCNT is 40 %. DI water, which was used as the base fluid, has a 999 kg/m3 density.

Specific heat capacity and density of the Al_2O_3 – MWCNT hybrid

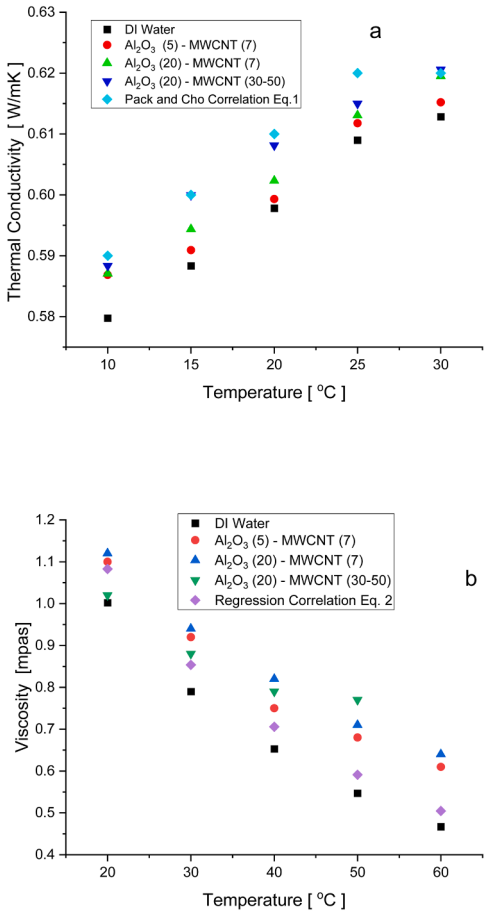

Fig. 3. a) Thermal conductivity and b) Viscosity of hybrid nanofluids.

nanofluids were estimated from the following mixture rules (Eqs. (5) and (6)), which are widely used in the literature, for example, Naik et al. [32].

Specific heat capacity and density are evaluated at bulk fluid temperature. This was by the work of Naik et al. [32].

$$\rho_{hnf} = (1-\varphi)\rho_{bf} + \varphi\rho_p \tag{5}$$

$$c_{hnf} = (1-\varphi)c_{bf} + \varphi c_p \tag{6}$$

where ρ_{hnf} , c_{hnf}, φ, ρ_{bf}, c_{bf} , c_p *and* ρ_p are the hybrid nanofluids Density, heat capacity (specific), volume concentrations, base fluid density (DI water), the specific heat capacity of the DI water (base fluid), the specific heat capacity of the hybrid nanoparticles, and density of the hybrid nanoparticles.

2.4. Experimental setup

Fig. 5 shows the basic design of the experimental setup. The Force convection test setup Consists of a storage tank (8) that can store and supply ten litres of water / Nanofluid for use during testing via a magnetic gear pump with variable speed (1). The power supply was attached to the test section to create a consistent heat flux along the test section to heat the fluid (Nanofluid or water) from T_i to T_e. The test section was well insulated with insulation material with a thickness of 70 mm and comprised of six layers to prevent the heat from being lost. The fluid left the test section through the Coriolis flow meter, which, when operating at full scale, had 0.05 % accuracy. Two flow meters were used, which have different flow ranges CmFs015, which has a range of 0.204 kg/min to 4.09 kg/min, and CmFs010, which is used to measure low flow rate operate between the range 0.068 kg/min to 1.36 kg/min, (4), a Heat

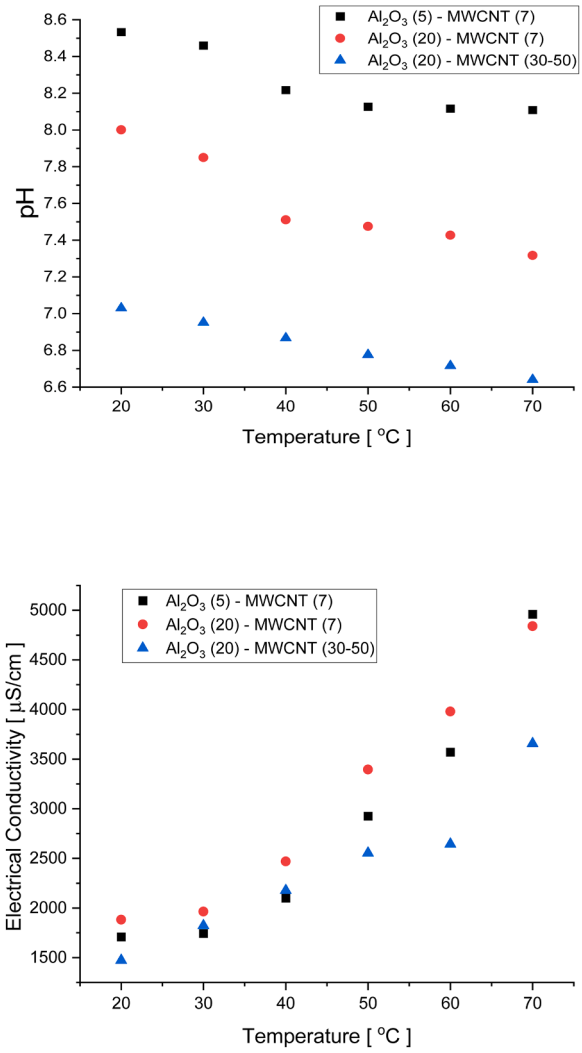

Fig. 4. a) pH value and b) Electrical conductivity of hybrid nanofluids.

exchanger (5) was used to cool the hot the fluid (Heated fluid from the Test sections (3)) where the heat was absorbed by water from a Thermal bath (6), the temperature at the input to the test section was kept constant. The system was equipped with a data-capturing device that collects information/signals from the power supply, flow meters, thermocouples, and pressure transducers and processes them in a computer (9). Data was logged using a Lab View application designed to log in at 20 Hz.

2.5. Test section

The test portion used in this study is depicted in Fig. 6. The test part comprised two mixers, a heat transfer test section, and a 500 mm hydrodynamic entrance section. The heated part of the test sections is a 1 m copper tube with internal and external diameters of 8.00 mm and 9.50 mm, respectively. The test area was insulated with six layers of insulation material to prevent heat loss from the heated section. A Constantine heating wire was used to heat the heat transfer test section at 217.8 W (Re ≈8.67 kW/m^2) using a DC power supply at 180 V and a current of 1.21A. 28 T-type thermocouples were evenly positioned throughout the test section wall at seven thermocouple positions, each with four thermocouples to measure the wall temperatures. These thermocouple positions were mounted on the test tube at 120, 250, 380, 510, 640, 770, and 900 mm from the inlet. To do this, a tiny pilot hole was drilled into the test portion, and a drop of solder was used to fasten

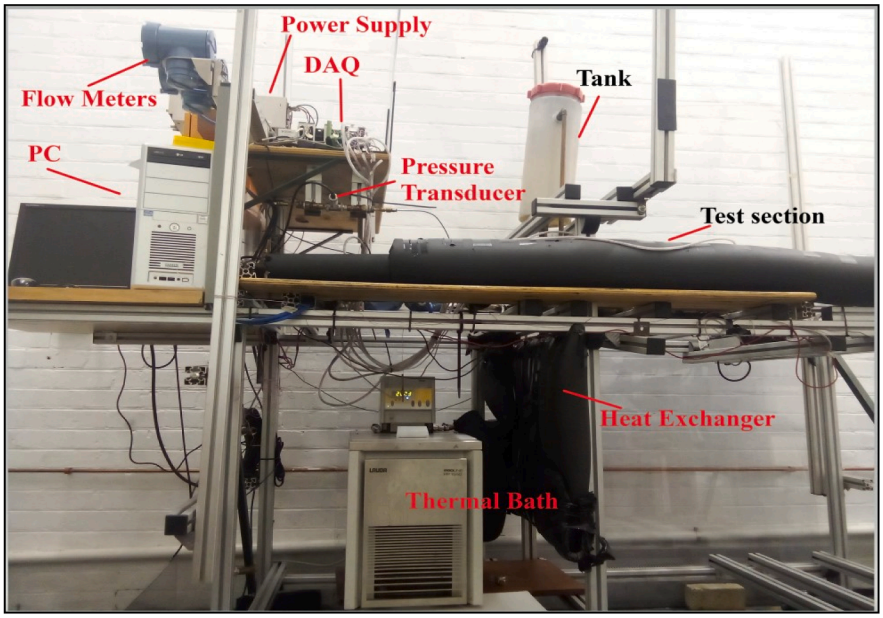

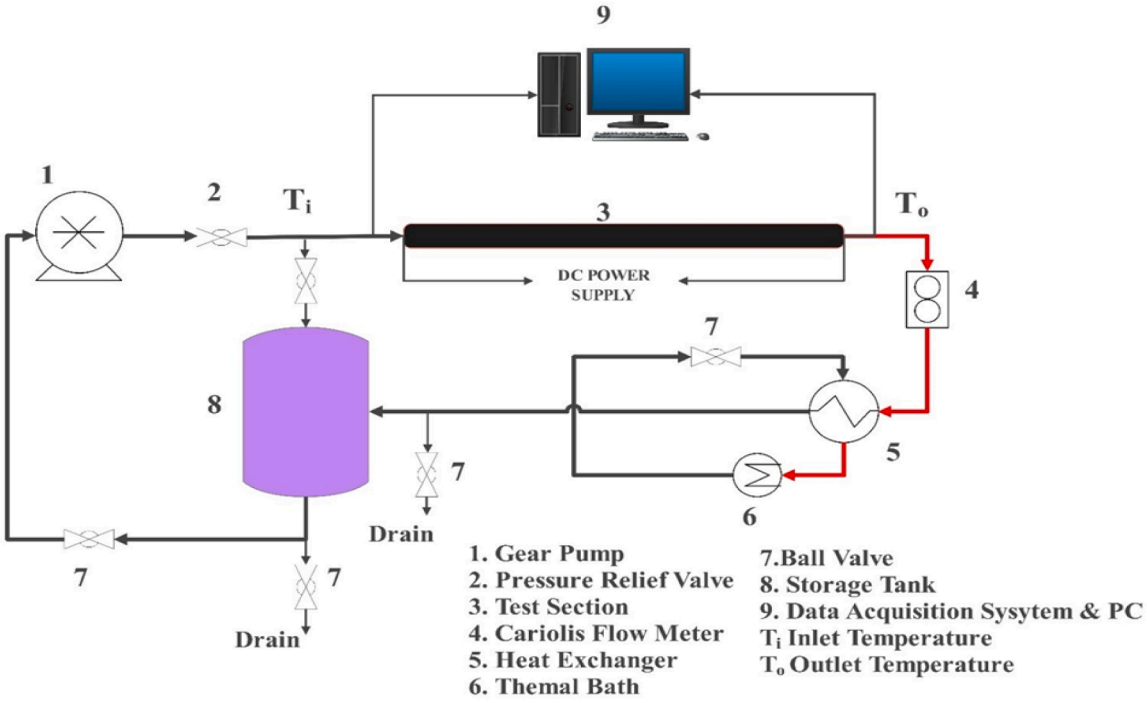

Fig. 5. Picture and the Schematic diagram of the experimental setup.

the thermocouple securely on the tube. A gap of about 1 mm between the thermocouple's positions and the tightly coiled Constantine wire was kept to maintain the constant supply of heat flux without interfering with the readings of the thermocouples. A similar process and gap were also maintained in the work of Evert et al. [29]. Two T-type thermocouples were situated at the tube inlet and outlet (test section) to record the inlet and outlet temperature. All these thermocouples were calibrated to within the accuracy of 0.1 °C. Fig. 7

2.6. Experimental procedure

The system was allowed to stabilise for at least one and a half hours after starting up to reach steady-state conditions. A steady state is believed to have been reached when there are no visible changes in the temperature, flow rate, and pressures. After the system reached a steady state, minor adjustments were made to the flow rates to attain the desired new flow rate for data collection. For every mass flow rate change (i.e., from a higher flow rate to a lower flow rate), it takes about 10 min for the system to return to its steady state. Data were captured from the high flow rate to the lower flow rate to prevent any residual heat from being stored in the insulation and affecting the subsequent reading. For every data point analysis, two hundred readings were recorded by the data acquisition systems, and the average value was used.

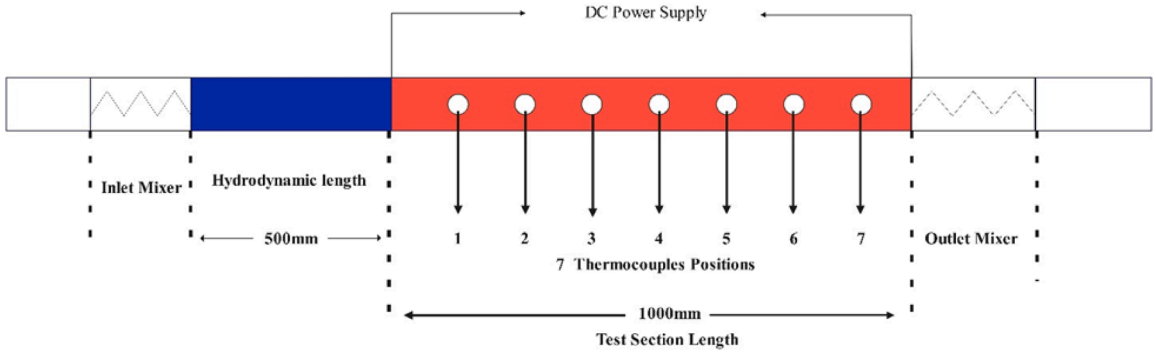

Fig. 6. Schematic diagram of test section.

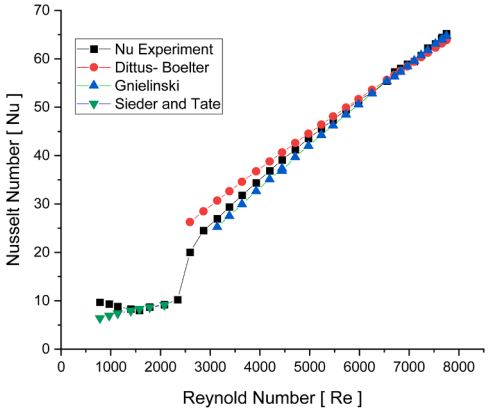

Fig. 7. Validations of the experimental measurements and data with the correlations.

2.7. Data reduction

The fluid local convective heat transfer coefficient $h(x)$ was calculated using Newton's cooling law, as given by Eq. (7). [45]

$$h(x) = \frac{\dot{q}}{T_{si}(x) - T_f(x)} \tag{7}$$

Where $\dot{q}$ is the heat flux obtained from the energy supplied to the system.

Energy supplied from the Heater (input) $\dot{Q}_e$

$$\dot{Q}_e = VI \tag{8}$$

Then, heat flux $\dot{q}$ is calculated as given in Eq. (9).

$$\dot{q} = \frac{\dot{Q}_e}{A_S} \tag{9}$$

The internal surface area of the tube (surface area) A_S

$$A_S = \pi DL \tag{10}$$

The heat flux of 8.67 kW/m^2 supplied to the system remains constant throughout the experiment.

The local inner surface temperatures ($T_{si}(x)$) and ($T_f(x)$) were obtained from the measured value of the outside wall temperature, ($T_{so}(x)$) measured by thermocouples, and resistance through the tube material (R_m), as shown in Eq. (11).

$$T_{si}(x) = T_{so}(x) - \dot{q}R_m \tag{11}$$

Where R_m is given in Eq. (12).

$$R_m = \frac{\ln \frac{D_o}{D_i}}{2\pi k_{cu} L} \tag{12}$$

k_{cu} is the thermal conductivity of the copper and is calculated as defined by Abu-Eishah [47] and applied by Meyer et al. [31]. The mean fluid temperature T_f was obtained from the relations given in Eq. (13).

$$T_f(x) = T_i + \frac{\dot{q}xp}{\dot{m}c_p} \tag{13}$$

The average convective heat transfer coefficient h_{avg} was obtained by taking the average of the above equations along the tube length at all the seven thermocouples' positions as given by Eq. (14).

$$h_{avg} = \frac{(h(x_1) + h(x_2) + h(x_3) + \ldots\ldots h(x_n))}{n} \tag{14}$$

where $n = 7$.

Reynold number (Re) and Prandtl number (Pr) of the working fluid were determined from the following relations (Eqs. (15) and (16)).

$$\mathrm{Re} = \frac{4\dot{m}}{\pi DiL} \tag{15}$$

$$\mathrm{Pr} = \frac{\mu c_p}{k} \tag{16}$$

The average value of the Nusselt number (Nu) was computed from the heat transfer coefficient, (Average h(x)) h_{avg}

$$Nu_{avg} = \frac{h_{avg}D_i}{k} \tag{17}$$

k Denotes the thermal conductivity of the fluids. For water, the thermal conductivity was determined at fluid bulk temperatureT_b.

Meanwhile, the Colburn – j factor (j) and friction factors were obtained from Eqs. (18 and 19). Table 2

$$j = \frac{Nu}{\mathrm{RePr}^{\frac{1}{3}}} \tag{18}$$

$$f = \frac{\Lambda P \rho D_i^5 \pi^2}{8(\dot{m})^2 L(x)} \tag{19}$$

Table 2
Experimental condition and parameters for the experiments.

Parameters	Symbols	Value / Ranges
Internal Diameter	D_i	8mm
External Diameter	D_o	9.5mm
Length of the Test section	L	1000mm
Heat Flux	$\dot{q}$	8.67 kW/m^2
Reynold Numbers	Re	1000 - 5000
Inlet Temperature (i.e., Nanofluid)	T_i	23 ^{O}C
Mass flow Rate [kg/s]	$\dot{m}$	0.0057 – 0.032 kg/s

2.8. Uncertainty analysis

Uncertainties of this experimental data were estimated within a 95 % confidence interval, using a similar method used by Osman et al. [34] and Everts et al. [48], and this method was adopted from the work of Dunn et al. [49]. Some important equations used for this analysis were given in Eqs. (20)–22. Table 3 provides the list of the measuring instruments and their uncertainties. Uncertainties were evaluated at higher and lower Reynold numbers of 4600 and 1000, a similar approach was used by Meyer et al. [31] and Osman et al. [34]. At high Reynold number of 4600, Nusselt number (Nu), coefficient of heat transfer (h), and Reynold number (*Re*) uncertainties were found to be 8.9%, 6.7 %, and 11 %, respectively. While at the low Reynold number of 1000, the uncertainties were 5.8 %, 7.2 %, and 9.82% for the Nusselt number (Nu), coefficient of heat transfer (h), and Reynold number, respectively.

$$\delta Nu = \left[\left(\frac{\delta Nu}{\delta h}\delta h\right)^2 + \left(\frac{\delta Nu}{\delta D}\delta D\right)^2 + \left(\frac{\delta Nu}{\delta k}\delta k\right)^2\right]^{1/2} \tag{20}$$

$$\delta h = \left[\left(\frac{\delta h}{\delta \dot{q}}\delta \dot{q}\right)^2 + \left(\frac{\delta h}{\delta T_S}\delta T_S\right)^2 + \left(\frac{\delta h}{\delta T_b}\delta T_b\right)^2\right]^{1/2} \tag{21}$$

$$\delta \mathrm{Re} = \left[\left(\frac{\delta \mathrm{Re}}{\delta \dot{m}}\delta \dot{m}\right)^2 + \left(\frac{\delta \mathrm{Re}}{\delta D}\delta D\right)^2 + \left(\frac{\delta \mathrm{Re}}{\delta A_c}\delta A_c\right)^2\right]^{1/2} \tag{22}$$

2.7. Validations of experimental setup and results

Water was used to validate this experimental setup by performing measurements in the laminar and turbulent flow regimes. In this current study, experimental data of Nusselt number was compared with verified correlations as available in the textbook by Cengel and Ghajar [50]. Experimental results along the turbulent region are compared with the correlations of Gnielinski and Dittus – Boelter [50]. Gnielinski correlation was found to underpredict the result within 3 % in the turbulent regime. Dittus – Boelter correlation was also found to validate this experimental data in the turbulent region, results shows that, the correlation (i.e., Dittus Boelter correlation) over predicts the experimental results within 2 %. Similar findings with Dittus Boelter correlation were also reported within the Reynold number ranges of $2500 \leq Re \geq 10{,}000$ in the literature [51–57]. In contrast, in the laminar region, Siede and Tate's correlation [50] correlates very well with the experimental data in the region. The correlation underpredicts the results with an average deviation of 9.0 %. This confirms the correctness of the measuring approach and validates the experimental data reduction procedure.

Table 3
Measuring instruments and their uncertainties.

Measuring instruments	Make / Type	Specifications/ Range	Uncertainty
Thermocouples	T – Type Thermocouples	−250 °C to 400 °C	0.1 °C
Flow meters	Coriolis flowmeter CmFs015 CmFs010	0.204 kg/min - 4.09 kg/min 0.068 kg/min - 1.36 kg/min	0.1%
Pressure Transducers	Omega 10WDWUI	0 - 17 Kpa	0.25 %
Power Supply Voltage Current	KIKUSUI PWR800M	0- 320 V 0- 12.5 A	0.33 V 0.04 A
Thermal Conductivity	KD2 Pro-Thermal conductivity meter	Controller: 0 to 50 °C Sensor; - 50 to +150oC	5 % from 0.2 to 2 W/mK and 0.01 from 0.02 to 0.2 W/mK
Viscosity	Sv–10 Vibro Viscometer (A&D, Japan),	Range; 0.3 - 10,000 mPa·s Operating Temperature: 10 - 40 °C	Less than 1 % at Full scale
pH Meter	H198129 / H198130 Waterproof pH COMBO. Henna Instruments	0 - 4000 $\mu s/cm$	0.05
Electrical conductivity	CON 700 conductivity meter	0 µS to 200.0mS	1%

3. Results and discussion

3.1. Effects of particle sizes on Coburn j factors

Fig. 8 shows the graph of Colburn j factor as a function of Reynold number for all the three nanofluids and DI water. The figure shows how the transitional flow regime appeared to have started at a different Reynold numbers. It's worth noting that these nanofluids are of the same volume concentration (i.e., 0.3 %). They only differ from the combination of nanoparticle sizes in the hybrid mixture. (i.e., Al_2O_3 (20) – MWCNT(30–50), Al_2O_3 (5) – MWCNT(<7), Al_2O_3 (20) – MWCNT(<7)).

Apart from pictorially showing how the transition ranges of the three fluids differ, it also presents the effects of the fluid thermophysical properties on the Colburn J factor. Results from the thermophysical properties of these hybrid nanofluids (i.e., Fig. 3), have shown that both thermal conductivity and viscosity were affected as the particle sizes varied. These effects were visibly noticed in the fluid heat transfer characteristics presented in Figs. 8 and 12. From Fig. 8 It can be seen that Al_2O_3 (20) – MWCNT(<7) nanofluid have the highest Colburn j factor, followed by Al_2O_3 (5) – MWCNT(<7) and Al_2O_3 (20) – MWCNT(30–50) respectively. But by comparing with Fig. 3, it can be concluded that Colburn J factors were more affected by viscosity. This may be due to the influence of viscosity on the Prandtl number. Because in Fig. 3, Al_2O_3 (20) – MWCNT(<7) nanofluid has shown a slightly higher viscosity. Therefore, at a particular Reynold number, fluid with high viscosity tends to have a high colburn j value. This can be seen clearly when nanofluids are compared with the base fluid (i.e., DI water).

3.2. Start of the transition flow regime

One of the ways to determine the start of the transitional regime is by using the critical Reynold number (Re_{cr}), as explained by Cengal et al. [50]. To identify the Re_{cr} for the three nanofluids and water, a similar method used by Everts and Meyer [27] was used. This method was adopted from the work of Ghajar and Tam [58] as given by Eq. (23).

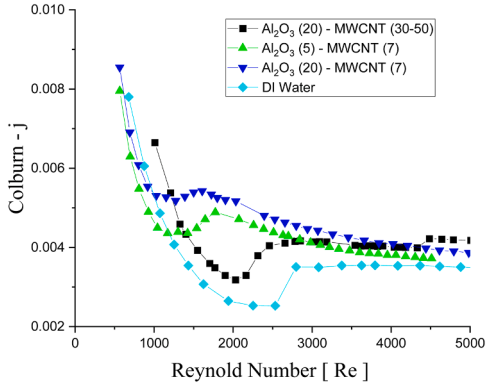

Fig. 8. Colburn j factor as the function of Reynold for the three nanofluids and water.

$$\mathrm{Re} = \mathrm{Re}_{cr}, \text{When Re} = \left(\frac{dj}{d\mathrm{Re}}\right) = 0 \quad (23)$$

The start of the transition or the point where transition starts in a tube flow has not been the same or constant, even though it was widely accepted in the literature to be at $Re = 2300$ [59]. Research shows that there are several reasons that affect the start and end of the transition regime. However, no work is reported in the literature investigating the factors that influence the start or end of the transition regime using nanofluids, more especially hybrid nanofluids. Neither the effect of nanoparticles on the start or end of the transition regime in a tube was investigated. Nonetheless, several works investigate the start of the transition regime in a tube with water as a working fluid. For example, Meyer and Oliver [59] explained that transition is affected by several parameters, which includes type of tubes (i.e., smooth tube or rough tube) and inlet configurations. It was found that transition is delayed mostly (i.e., Delayed start) in smooth tubes, while it occurs early in rough tubes [59,60]. Nagendra et al. [61], in one of the earlier works on the transitional flow regime, explained that the greater the disturbance along the tube, the earlier the transition occurs. So, the critical question is, as nanofluids contains nanoparticles, can the dispersed nanoparticles affect the start of the transition flow? To answer this question experimentally, it is important to look critically at the literature on the reported factors that affect the start of the transition and its range, then the present results can be analysed better. Ghajar and Madon [30] investigated the influence of three different inlet configurations, i.e., an inlet with sudden contractions (i.e., Square-edged) and a tube protruding square-edged inlet called a re-entrant inlet and a bell-mouth inlet (smooth, gradual contraction). It was found that the start of the transitioning from laminar to turbulent flow occurs at different critical Reynold numbers (Re_{cr}) for the three inlets evaluated. This shows how the transition regime depends on inlet configuration. Effects of tube roughness, free convections, use of inserts, the heating method, and roughness height were also reported to influence the transition flow range significantly [62–65]. According to Eq. (23), the critical Reynold number (Re_{cr}) of Al_2O_3 (20) – MWCNT(30–50) nanofluid is evaluated and presented in Fig. 9a (i.e., The nanofluid with the bigger particle sizes combination) and transition appeared to have started at the $Re_{cr} = 1898.5$. Fig. 9b shows that transition was found to start at $Re_{cr} = 1172$ for Al_2O_3 (5) – MWCNT(<7). While Al_2O_3 (20) – MWCNT(<7) nanofluid (i.e., Fig. 9c), and DI water (i.e., Fig. 9d) transition begins at the $Re_{cr} = 1150$ and 2077 respectively.

These results demonstrate how nanoparticles dispersed in the base fluid have affected the start of the transitional flow regime. It also became more apparent that the dispersed nanoparticles have contributed to an increase in the disturbances in the flow, which resulted in the occurrence of the transition much earlier than in the base fluid. A study by Nagendra et al. [61] also confirmed that the greater the disturbance along the tube, the earlier the transition occurs. Therefore, the dispersion of these nanoparticles in the base fluids increased the fluid flow disturbances, resulting in the transition's early starts. In this study the transition was delayed for Al_2O_3 (20) – MWCNT(30–50) nanofluid, then with Al_2O_3 (5) – MWCNT(<7), followed by Al_2O_3 (20) – MWCNT(<7) nanofluid. When compared with the base fluid (DI water), transitions appeared to have started earlier with the nanofluids than with the base fluid.

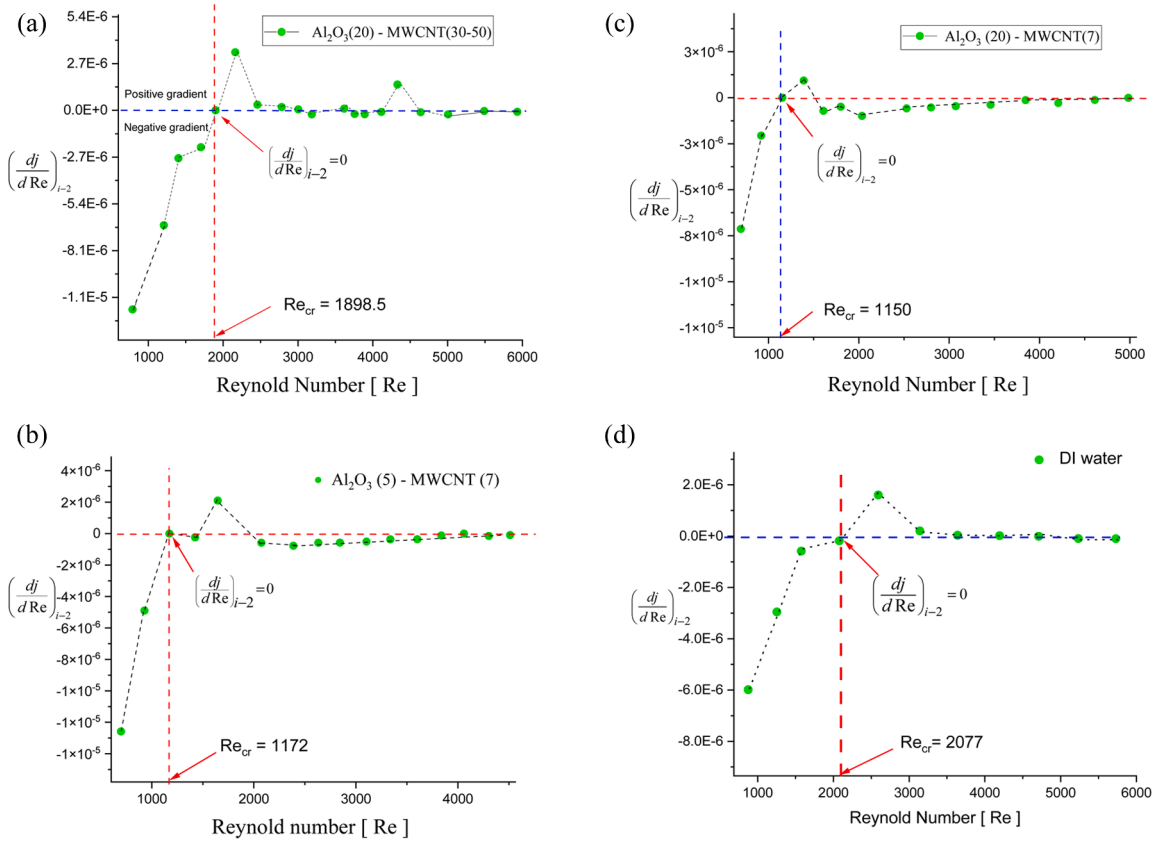

Fig. 9. a. The gradient of Colburn j factor as a function of Reynold number to identify the Re_{cr} at which the transition starts for Al_2O_3 (20) – MWCNT(30–50) nanofluid.
b. A gradient of Colburn j factor as a function of Reynold number to identify the Re_{cr} at which the transition starts for Al_2O_3 (5) – MWCMT(7) nanofluid.
c. A gradient of Colburn j factor as a function of Reynold number for identifying the Re_{cr} at which the transition starts for Al_2O_3 (20) – MWCNT(<7) nanofluid.
d. A gradient of Colburn j factor as a function of Reynold number for identifying the Re_{cr} at which the transition starts for base fluid (DI -Water).

3.3. Range of transitional flow regime (ΔRe)

To find the range of the transitional flow regime, it is necessary to identify the Reynolds number to which the turbulent flow starts. Cengal et al. [50] explained that the beginning of the turbulent flow can be determined by comparing the experimental results of Nusselt number or Colburn J factor values with turbulent correlation. Using this approach provided by Cengal et al. [50] and Everts and Meyer [27,66], it was possible to come up with the values of the Reynold number to which the transitional flow regime ends and the start of the turbulent regime. In this study, we compared the results with the correlations of Maiga et al. [67] and the Dittus – Boelter correlation [50] (Eqs. (24) and (25)), but Dittus - Boelter correlation (i.e., Eq. (25)) gives a better comparison and is presented in Fig. 10. The correlation of Dittus - Boelter (i.e., Eq. (25)) correlates better with the experimental data of hybrid nanofluids in the turbulent region. It validates the experimental results of Al_2O_3 (20) – MWCNT(<7) nanofluid with an average deviation of 16 %, while Al_2O_3 (20)–MWCNT(30–50) and Al_2O_3 (5) – MWCNT(<7) with an average deviation of 14% and 18 % respectively. Therefore, using Eq. (25), we come up with an approximate or estimated Reynold number to which the turbulent flow starts.

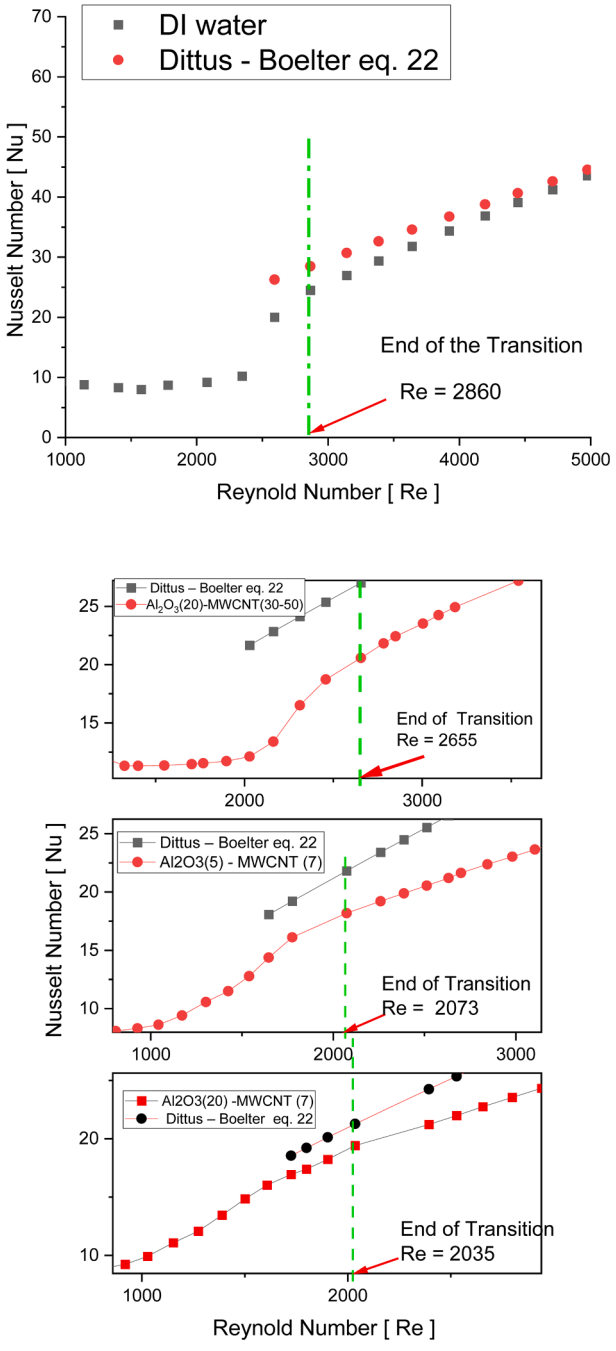

Fig. 10. End of the transitional regime for the base fluid (DI- Water) and three nanofluids.

$$Nu = 0.085\mathrm{Re}^{0.71}\mathrm{Pr}^{0.35} \quad (24)$$

$$Nu = 0.023\mathrm{Re}^{0.8}\mathrm{Pr}^{0.4} \quad (25)$$

To appropriately compare the nanofluid and base fluid, a similar approach was followed to come up with the end of the transition for the base fluid as shown in Fig. 10. From the results it was found that the transition ends at the Reynold number of 2860 for the base fluid.

This study found that the range of the transition regime for these three hybrid nanofluids varied significantly. This also proved the influence and impact of nanoparticles and their sizes on the hybrid nanofluids heat transfer characteristics. Table 4 summarises the results of transition regimes for the three hybrid nanofluids and base fluid used in this study.

Table 4 clearly shows the influence of the nanoparticles sizes on the transitional flow regime. As both fluids behave differently within the flow regime. These findings makes it clear that, dispersing of these nanoparticles not only improves the heat transfer characteristics of the base fluid but also influences other essential flow characteristics that are very significant, especially when designing heat exchangers. Fig. 11 (a – d) shows the flow regime boundaries for the nanofluids and DI water evaluated from the present experimental data.

3.4. Convective heat transfer characteristics

Convective heat transfer performances for these three hybrid nanofluids were also investigated. The fluids (i.e., Al_2O_3 (20) – MWCNT (30–50), Al_2O_3 (5) – MWCNT(<7), and Al_2O_3 (20) – MWCNT(<7)) were found to behave differently as regards to the heat transfer enhancement. Fig. 12a shows Al_2O_3 (20) – MWCNT(<7) nanofluids performed exceptionally well across all regimes except the laminar regime. Because together with Al_2O_3 (5) – MWCNT(<7), they have recorded a very low enhancement as compared to water. Nonetheless, across the transition regime, the Nusselt number (i.e., Nu) was found to increase by 48.86 % for Al_2O_3 (20) – MWCNT(<7) nanofluid. While for the other two nanofluids (i.e., Al_2O_3 (5) – MWCNT(<7) and Al_2O_3 (20) – MWCNT (30–50)) Nusselt number showed an enhancement of about 37.06 % and 37.55 %, respectively. Therefore, it can be suggested that for the hybrid nanofluid of Al_2O_3 and MWCNT, it is better to use a smaller particle size of the MWCNT. Because fluid with MWCNT (<7) nanoparticles exhibited better heat transfer enhancement compared to other sizes Fig. 12a. Another important aspect that is worth noting, because of it influence on the heat transfer performance and characteristics is the Brownian motion. The research work of Manay et al. [68] and Fani et al. [69] shows that Brownian motion significantly influences nanofluid heat transfer enhancement. Its impact were found to be deteriorating with the increase in nanoparticle sizes. According to Fani et al. [69], the probability of particle collision decreases with the increase in particle sizes. This leads to the decrease in Brownian motion effects and, as such, results in

Table 4
Summary of the transitional flow data for the three fluids and water.

Nanofluids and Base Fluid	Particle sizes (nm)		Transition flow regime (*Re*)	
	Al_2O_3	MWCNT	Start	End
$Al_{2O3(20)-MWCNT(30-50)}$	20	30–50	1898.5	2655
$Al_{2O3\ (5)\ -\ MWCNT(<7)}$	5	7	1172	2073
$Al_{2O3\ (20)\ -\ MWCNT(<7)}$	20	7	1150	2035
DI Water	–	–	2077	2860

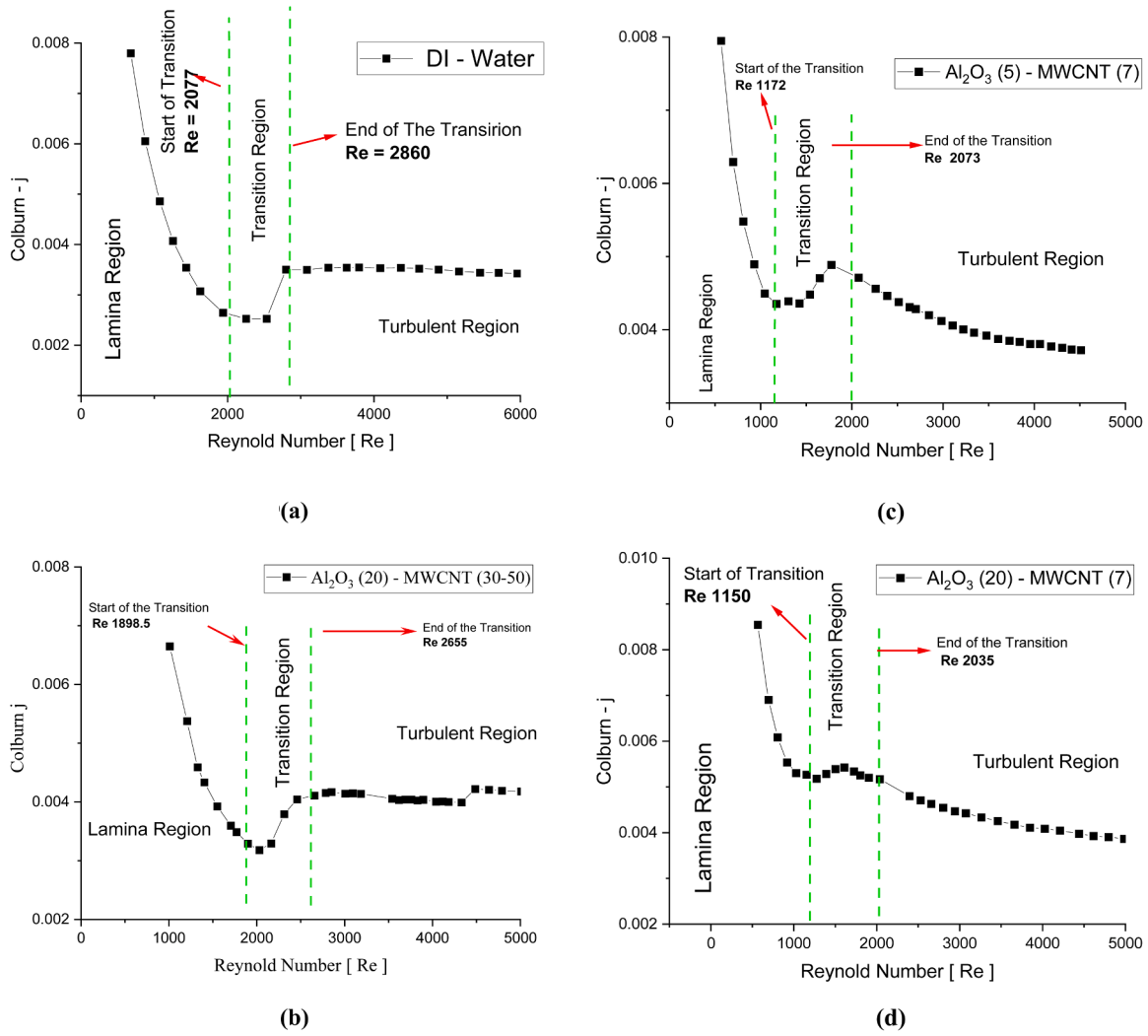

Fig. 11. Colburn-J factor versus *Re* for identification of lamina, transition, and turbulent regions for (a) DI water, (b) Al_2O_3 (20) – MWCNT(30–50), (c) Al_2O_3 (5) – MWCNT(<7), (d) Al_2O_3 (20) – MWCNT(<7).

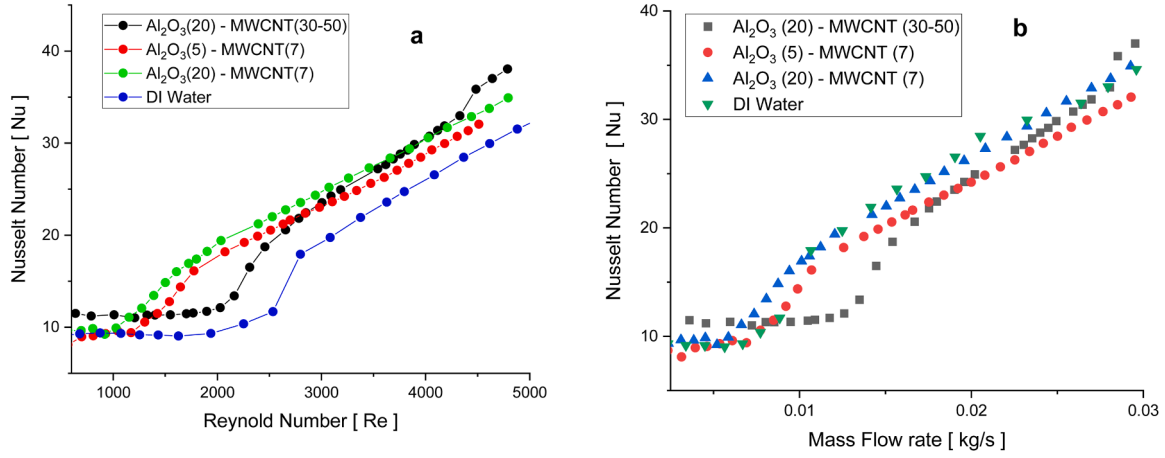

Fig. 12. a) Variations of Nusselt number with Reynold number **b)** Variations of Nusselt number with mass flow rate for DI water and three hybrid nanofluids.

the reduction of heat transfer enhancement of the nanofluids [69]. These findings agreed with the results of this research, because Al_2O_3 (20) – MWCNT (30–50) (i.e., fluid with much bigger particle sizes) have the lowest enhancement in Nusselt number compared to the other two nanfluids. But Al_2O_3 (5) – MWCNT (<7) appeared to behave contrary to the findings of Fani et al. [69]. Because Al_2O_3 (5) – MWCNT (<7) nanofluid have less heat transfer enhancement than Al_2O_3 (20) – MWCNT (<7), despite having much smaller particle sizes. But Manay

et al. [68] explained that thermophoresis, is highly related to the Brownian motion. The same opinion was also shared with Haddad et al. [70] and Sheikholeslami et al. [71].. Also the research work of Neild et al. [72] and Fani et al. [69] found that the combined effects of thermophoresis and Brownian motion reduce Nusselt number. So, at this point, it will be tough to make conclusions on the effects of Brownian motion and thermophoresis on the heat transfer enhancement of these nanofluids. Because despite the significance of these phenomena (i.e., Brownian motion and thermophoresis), there are other critical factors which are equally important and were found to influence the heat transfer characteristics of nanofluids. Factors like the Dufour effect, buoyancy-induced secondary flow (natural or mixed convection effects), etc., and are very important on nanofluids heat transfer characteristics.

Fig. 12b shows the effects of mass flow rate on particle sizes. Results show that nanofluids heat transfer enhancement deteriorates compared to the base fluid. A similar finding was also reported by Meyer et al. [31] when they compared heat transfer coefficient as a function of fluid velocity for MWCNT – Water nanofluid. The same results were also reported by Pak and Cho [73] and Yu et al. [74].. This was due to the disparity of their viscosity, where nanofluids have a much higher viscosity than the base fluids [73,74]. However, comparing the three fluids based on the effects of particle sizes as a function of mass flow rate, similar findings to Fig. 12a were noticed. Al_2O_3 (20) – MWCNT (30–50), have shown the most minor performance as compared to the Al_2O_3 (20) – MWCNT (<7) and Al_2O_3 (5) – MWCNT (<7), nanofluids in the transition region.

3.5. Effects on pressure drops, thermal efficiency, and thermal performance coefficient

Other important heat transfer properties that were affected by the variation of particle sizes are Thermal efficiency, pressure drop, and friction factors. Similar findings were also reported by Meriläinen et al. [75], where effects of particle sizes were investigated for different single nanofluids of Al_2O_3 - water, SiO_2 - water, and MgO - water nanofluids in the turbulent regime. Table 5 shows the thermal efficiency, pressure drop, friction factor, and Coefficient of thermal performances at a transitional Reynold number of $Re \approx 2000$. This position was chosen because it is the Reynold number that falls within the transition range of all three fluids. This was similar to the method used by Anoop et al. [38]. Where heat transfer performance and particle size effects of Al_2O_3-water nanofluid are analysed at laminar Reynold number of 1500 [38]. Thermal efficiencies for the three hybrid nanofluids were computed according to Eq. (23), which was in accordance to the work of Goharkhah et al. [76] and Mehrali et al. [77]. However, the pressure drops and friction factors were also noticed to have varied, and they are very critical to the nanofluids heat transfer performance. Therefore, Eq. (24) was used to compute the coefficient of thermal performance (COP) of the hybrid nanofluid. This was in accordance with Nadooshan et al. [41], Goharkhah et al. [76] and Meriläinen et al. [75].

Table 5
Comparison of the effect of particle sizes on pressure drops and thermal efficiency at $Re \approx 2000$.

S/N	Nanofluid	Pressure drops (kPa)	Friction factor	Thermal Efficiency	Thermal performance coefficient
1	Al_2O_3(20) –MWCNT (30–50)	0.166	0.0420	1.100	0.869
2	Al_2O_3(5) –MWCNT (<7)	0.180	0.0459	1.655	1.202
3	Al_2O_3(20) –MWCNT (<7)	0.157	0.0435	1.772	1.539

$$\eta = \frac{h_{hnf}}{h_{bf}} \tag{26}$$

$$\frac{h_{hnf}/h_{bf}}{\left(P_{pumping}\right)_{hnf}/\left(P_{pumping}\right)_{bf}} \tag{27}$$

From Table 5, results show that Al_2O_3 (20) –MWCNT (<7) nanofluid have the highest thermal efficiency, followed by Al_2O_3 (5) – MWCNT (<7), and Al_2O_3 (20) –MWCNT (30–50), respectively. Fig. 13 also notes that Al_2O_3 (5) –MWCNT (<7) nanofluid has the highest pressure drop and friction factor among all three fluids. However, its thermal efficiency and coefficient of thermal performance (COP) were better than those of Al_2O_3(20) –MWCNT (30–50). This was similar to the findings reported by Meriläinen et al. [67], where SiO_2 – water nanofluid (with 6.5 nm particle size) at 0.02 % and 0.03 % volume concentration have shown higher friction factor and convective heat transfer efficiency than SiO_2 – water nanofluid (with 28–110 nm particle size). According to Nadooshan et al. [41], a fluid has higher positive energy efficiency if its coefficient of thermal performance is more than one. Results in Table 5, have shown that Al_2O_3(20) –MWCNT (<7) and Al_2O_3(5) –MWCNT (<7) all have a coefficient of thermal performance that is greater than 1, with values of 1.539 and 1.202, respectively. While Al_2O_3(20) –MWCNT (30–50), nanofluid has the lowest value, with a value of 0.869. This shows that Al_2O_3(20) –MWCNT (<7) nanofluid has shown the best heat transfer properties in terms of Nusselt number enhancement, thermal

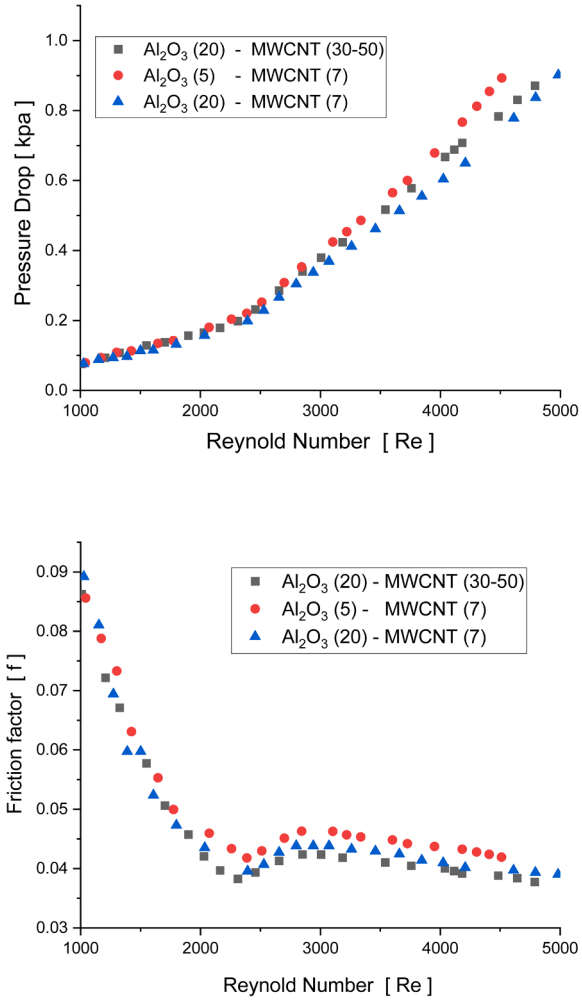

Fig. 13. a) Variation of pressure drop with Reynolds number, b) Variation of Friction factor with Reynolds number.

efficiency, and coefficient of thermal performance (COP) as compared to the other two fluids.

Fig. 13 presents the pressure drop and friction factor variation with the Reynold number along the lamina, transition, and turbulent regimes. Even though this research focuses primarily on the transition region, it is interesting to highlight the key findings. Results show that Al_2O_3(5) –MWCNT (<7) nanofluid has the highest pressure drop and friction factor across all the flow regimes. It was also noticed that, the difference in the friction factor and pressure drops between the three hybrid nanofluid fluids is more significant in the turbulent region than in the laminar region. This finding was consistent with the results reported by Meriläinen et al. [75].

4. Conclusions

A forced convective heat transfer experiment was conducted with hybrid nanofluids of Al_2O_3 and MWCNT inside a copper tube, which is heated at a constant heat flux of 8.67 kw/m^2. In this study, the main aim was to examine the influence of particle size on the heat transfer characteristics along the transition regime. Two particle sizes for Al_2O_3 and MWCNT were used to prepare three hybrid nanofluids with different particle size combinations (i.e., Al_2O_3 (20) – MWCNT(30–50), Al_2O_3 (5) – MWCNT(<7), Al_2O_3 (20) – MWCNT(<7)).

It is essential to point out that these observations were made from experimental data of a hybrid nanofluid with a percentage weight concentration of 60:40, which comprises 60 % Al_2O_3 and 40 % MWCNT. Since hybrid nanofluid properties changes when the percentage of each constituent particle changes, affecting both fluid thermal conductivity, density, and convective heat transfer characteristics. Therefore, these conclusions may not be extended and generalised to all hybrid nanofluids of Al_2O_3 – MWCNT. So these conclusions were specifically drawn from the experimental results, which are based on the 60:40 hybrid nanofluids of Al_2O_3 – MWCNT;

- It was observed that the heat transfer characteristics of the base fluid (DI water) were improved by dispersing the nanoparticles. Both particle size combinations have remarkably enhanced heat transfer coefficients, especially in transition and turbulent regions.
- Hybrid nanofluids with particle size combination 20 and <7 nm of Al_2O_3 and MWCNT have shown the best heat transfer performance along the transition flow regime. The Nusselt number was enhanced by 48.86 % along this region, while Al_2O_3(20) – MWCNT (30–50) and Al_2O_3(5) – MWCNT (<7) nanofluids have also shown an enhancement of Nusselt number by 37.5 % and 37.0 %, respectively.
- Results also show that fluid thermal efficiency, pressure drops, friction factor, and coefficient of thermal performance of the nanofluid also varied as the particle size combination changed. Hybrid nanofluid of Al_2O_3(20) – MWCNT (<7) has shown a much better heat transfer characteristic. It has the highest thermal efficiency (i.e., 1.772) and coefficient of thermal performance (i.e., 1.539) compared to the other fluids. It also had the lowest friction factor and pressure drop compared to the other hybrid nanofluids examined. The friction factor and pressure drop of Al_2O_3(20) – MWCNT (<7) nanofluid were lower than that of Al_2O_3(5 nm) – MWCNT (<7 nm) by 5.2 % and 12.78 % respectively.
- Furthermore, it was observed that the range of the Reynold number at which the transition occurs for the three nanofluids has also varied, indicating that the nanoparticle sizes significantly influence the transition regime. The three nanofluids also appeared to have different critical Reynold numbers. The critical Reynold numbers are 1152, 1172, and 1898 for Al_2O_3(20 nm) – MWCNT (<7 nm), Al_2O_3(5 nm) – MWCNT (<7 nm), and Al_2O_3(20 nm) – MWCNT (30–50) respectively.

CRediT authorship contribution statement

Ibrahim Umar Ibrahim: Writing – original draft, Investigation, Formal analysis, Data curation. **Mohsen Sharifpur:** Writing – review & editing, Validation, Supervision, Resources, Project administration, Methodology. **Josua P. Meyer:** Writing – review & editing, Supervision, Methodology, Funding acquisition. **S M Sohel Murshed:** Writing – review & editing, Methodology.

Declaration of competing interest

The authors declare that they have no known competing financial interests or personal relationships that could have appeared to influence the work reported in this paper.

Data availability

Data will be made available on request.

Acknowledgment

S.M.S. Murshed acknowledges Fundação para a Ciência e a Tecnologia (FCT) for its financial support via the project LAETA Base Funding (DOI: 10.54499/UIDB/50022/2020).

References

[1] M. Ghobadi and Y.S. Muzychka, "Heat transfer and pressure drop-in mini channel heat sinks," 10.1080/01457632.2015.965097, vol. 36, no. 10, pp. 902–911, Jul. 2014, 10.1080/01457632.2015.965097.
[2] I.U. Ibrahim, M. Sharifpur, O. Manca, J.P. Meyer, Nanofluid's convective heat transfer for laminar, transitional, and turbulent flow, Nanofluid Appl. Adv. Therm. Sol. (2023) 151–192, https://doi.org/10.1016/B978-0-443-15239-9.00006-0. Jan.
[3] E.C. Okonkwo, I. Wole-Osho, I.W. Almanassra, Y.M. Abdullatif, T. Al-Ansari, An Updated Review of Nanofluids in Various Heat Transfer Devices, Springer International Publishing, 2020, https://doi.org/10.1007/s10973-020-09760-2 no. April.
[4] I.U. Ibrahim, M.U. Kaisan, I.A. Hussain, Y.S. Dambatta, and A. Shitu, "Recent research on water management problem in proton exchange membrane fuel cells: a brief review," no. December, pp. 75–85, 2020.
[5] S.M.S. Murshed, K.C. Leong, and C. Yang, "Thermophysical and electrokinetic properties of nanofluids-a critical review," 2008, 10.1016/j.applthermaleng.2008.01.005.
[6] S.M. Sohel Murshed, C.A. Nieto De Castro, M.J.V. Lourenç, M.L.M. Lopes, F.J. V. Santos, A review of boiling and convective heat transfer with nanofluids, Renew. Sustain. Energy Rev. 15 (2011) 2342–2354, https://doi.org/10.1016/j.rser.2011.02.016.
[7] A. Kaggwa, J.K. Carson, Developments and future insights of using nanofluids for heat transfer enhancements in thermal systems: a review of recent literature, Int. Nano Lett. 9 (4) (2019) 277–288, https://doi.org/10.1007/s40089-019-00281-x.
[8] L.T. Carmichael, V. Berry, B.H. Sage, Thermal Conductivity of Fluids. Ethane, J. Chem. Eng. Data 8 (3) (1963) 281–285, https://doi.org/10.1021/je60018a001.
[9] X.Q. Wang, A.S. Mujumdar, Heat transfer characteristics of nanofluids: a review, Int. J. Therm. Sci. 46 (1) (2007) 1–19, https://doi.org/10.1016/j.ijthermalsci.2006.06.010.
[10] M.A. Sabiha, R.M. Mostafizur, R. Saidur, S. Mekhilef, Experimental investigation on thermo physical properties of single-walled carbon nanotube nanofluids, Int. J. Heat. Mass Transf. 93 (2016) 862–871, https://doi.org/10.1016/j.ijheatmasstransfer.2015.10.071.
[11] Y. Wang, H.A.I. Al-Saaidi, M. Kong, J.L. Alvarado, Thermophysical performance of graphene-based aqueous nanofluids, Int. J. Heat. Mass Transf. 119 (2018) 408–417, https://doi.org/10.1016/j.ijheatmasstransfer.2017.11.019.
[12] M.T. Zafarani-Moattar, R. Majdan-Cegincara, Effect of temperature on volumetric and transport properties of nanofluids containing ZnO nanoparticles poly (ethylene glycol) and water, J. Chem. Thermodyn. 54 (2012) 55–67, https://doi.org/10.1016/j.jct.2012.03.010.
[13] M. Kole, T.K. Dey, Investigation of thermal conductivity, viscosity, and electrical conductivity of graphene-based nanofluids, J. Appl. Phys. 113 (8) (2013), https://doi.org/10.1063/1.4793581.
[14] M.H. Ahmadi, A. Mirlohi, M.A. Nazari, R. Ghasempour, A review of thermal conductivity of various nanofluids, J. Mol. Liq. 265 (2018) 181–188, https://doi.org/10.1016/j.molliq.2018.05.124.
[15] S. Murshed, K. Leong, C. Yang, Enhanced thermal conductivity of TiO 2-water based nanofluids, Int. J. Therm. Sci. 44 (2005) 66, https://doi.org/10.1016/j.ijthermalsci.2004.12.005.

[16] S.M.S. Murshed, K.C. Leong, C. Yang, Investigations of thermal conductivity and viscosity of nanofluids, Int. J. Therm. Sci. 47 (2008) 560–568, https://doi.org/10.1016/j.ijthermalsci.2007.05.004.
[17] S.M. Sohel Murshed and C.A. Nieto De Castro, "Superior thermal features of carbon nanotubes-based nanofluids-a review," 2014, 10.1016/j.rser.2014.05.017.
[18] A. Azari, M. Kalbasi, M. Derakhshandeh, M. Rahimi, An experimental study on nanofluids convective heat transfer through a straight tube under constant heat flux, Chin. J. Chem. Eng. 21 (10) (2013) 1082–1088, https://doi.org/10.1016/S1004-9541(13)60618-7.
[19] H. Akhavan-Zanjani, M. Saffar-Avval, M. Mansourkiaei, F. Sharif, M. Ahadi, Experimental investigation of laminar forced convective heat transfer of Graphene-water nanofluid inside a circular tube, Int. J. Therm. Sci. 100 (2016) 316–323, https://doi.org/10.1016/j.ijthermalsci.2015.10.003. Feb.
[20] E. Nourafkan, G. Karimi, J. Moradgholi, Experimental study of laminar convective heat transfer and pressure drop of cuprous oxide/water nanofluid inside a circular tube, Exp. Heat Transf. 28 (1) (2015) 58–68, https://doi.org/10.1080/08916152.2013.803178.
[21] M.H. Aghabozorg, A. Rashidi, S. Mohammadi, Experimental investigation of heat transfer enhancement of Fe2O3-CNT/water magnetic nanofluids under laminar, transient and turbulent flow inside a horizontal shell and tube heat exchanger, Exp. Therm. Fluid. Sci. 72 (2016) 182–189, https://doi.org/10.1016/j.expthermflusci.2015.11.011.
[22] Y. Ding, H. Alias, D. Wen, R.A. Williams, Heat transfer of aqueous suspensions of carbon nanotubes (CNT nanofluids), Int. J. Heat. Mass Transf. 49 (1–2) (2006) 240–250, https://doi.org/10.1016/j.ijheatmasstransfer.2005.07.009.
[23] L. Syam Sundar, M.T. Naik, K.V. Sharma, M.K. Singh, T.C. Siva Reddy, Experimental investigation of forced convection heat transfer and friction factor in a tube with Fe 3O 4 magnetic nanofluid, Exp. Therm. Fluid. Sci. 37 (2012) 65–71, https://doi.org/10.1016/j.expthermflusci.2011.10.004.
[24] L. Megatif, A. Ghozatloo, A. Arimi, M. Shariati-Niasar, Investigation of laminar convective heat transfer of a novel Tio2-carbon nanotube hybrid water-based nanofluid, Exp. Heat Transf. 29 (1) (2016) 124–138, https://doi.org/10.1080/08916152.2014.973974. Jan.
[25] M. Gupta, V. Singh, S. Kumar, N. Dilbaghi, Experimental analysis of heat transfer behavior of silver, MWCNT and hybrid (silver +MWCNT) nanofluids in a laminar tubular flow, J. Therm. Anal. Calorim. 142 (4) (2020) 1545–1559, https://doi.org/10.1007/s10973-020-09453-w. Nov.
[26] S. Suresh, K.P. Venkitaraj, P. Selvakumar, M. Chandrasekar, Effect of Al2O3–Cu/water hybrid nanofluid in heat transfer, Exp. Therm. Fluid. Sci. 38 (2012) 54–60, https://doi.org/10.1016/J.EXPTHERMFLUSCI.2011.11.007. Apr.
[27] M. Everts, J.P. Meyer, Heat transfer of developing and fully developed flow in smooth horizontal tubes in the transitional flow regime, Int. J. Heat. Mass Transf. 117 (2018) 1331–1351, https://doi.org/10.1016/J.IJHEATMASSTRANSFER.2017.10.071. Feb.
[28] J.P. Meyer, Heat transfer in tubes in the transitional flow regime, in: Proceedings of the 15th International Heat Transfer Conference, IHTC 2014, Begell House Inc., 2014, https://doi.org/10.1615/ihtc15.kn.000003.
[29] M. Everts, P. Robbertse, B. Spitholt, The effects of surface roughness on fully developed laminar and transitional flow friction factors and heat transfer coefficients in horizontal circular tubes, Int. J. Heat. Mass Transf. 189 (2022) 122724, https://doi.org/10.1016/J.IJHEATMASSTRANSFER.2022.122724. Jun.
[30] A.J. Ghajar, K.F. Madon, Pressure drop measurements in the transition region for a circular tube with three different inlet configurations, Exp. Therm. Fluid. Sci. 5 (1) (1992) 129–135, https://doi.org/10.1016/0894-1777(92)90062-A. Jan.
[31] J.P. Meyer, T.J. McKrell, K. Grote, The influence of multi-walled carbon nanotubes on single-phase heat transfer and pressure drop characteristics in the transitional flow regime of smooth tubes, Int. J. Heat. Mass Transf. 58 (1–2) (2013) 597–609, https://doi.org/10.1016/j.ijheatmasstransfer.2012.11.074.
[32] M.T. Naik, L.S. Sundar, Heat transfer and friction factor with water/propylene glycol-based CuO nanofluid in circular tube with helical inserts under transition flow regime, Heat Transf. Eng. 35 (1) (2014) 53–62, https://doi.org/10.1080/01457632.2013.810451.
[33] S.S. Chougule, S.K. Sahu, Comparative Study on Heat Transfer Enhancement of Low Volume Concentration of Al2o3-Water and Carbon Nano-Tube-Water Nano-Fluids in Transition Regime Using Helical Screw Tape Inserts, Exp. Heat Transf. 29 (1) (2016) 17–36, https://doi.org/10.1080/08916152.2014.926432.
[34] S. Osman, M. Sharifpur, J.P. Meyer, Experimental investigation of convection heat transfer in the transition flow regime of aluminum oxide-water nanofluids in a rectangular channel, Int. J. Heat. Mass Transf. 133 (2019) 895–902, https://doi.org/10.1016/j.ijheatmasstransfer.2018.12.169.
[35] S.O. Giwa, M. Momin, C.N. Nwaokocha, M. Sharifpur, J.P. Meyer, Influence of nanoparticles size, percent mass ratio, and temperature on the thermal properties of water-based MgO–ZnO nanofluid: an experimental approach, J. Therm. Anal. Calorim. 143 (2) (2021) 1063–1079, https://doi.org/10.1007/S10973-020-09870-X/FIGURES/23. Jan.
[36] M. Shahul Hameed, S. Suresh, R.K. Singh, Comparative study of heat transfer and friction characteristics of water-based Alumina–copper and Alumina–CNT hybrid nanofluids in laminar flow through pipes, J. Therm. Anal. Calorim. 136 (1) (2019) 243–253, https://doi.org/10.1007/s10973-018-7898-z. Apr.
[37] M. Shahul Hameed, S. Suresh, Convective heat transfer and pressure drop characteristics of Al2O3-CNT/water hybrid nanofluid in a straight circular tube under turbulent flow, J. Nanofluids 6 (4) (2017) 743–750, https://doi.org/10.1166/jon.2017.1370. Aug.
[38] K.B. Anoop, T. Sundararajan, S.K. Das, Effect of particle size on the convective heat transfer in nanofluid in the developing region, Int. J. Heat. Mass Transf. 52 (9–10) (2009) 2189–2195, https://doi.org/10.1016/j.ijheatmasstransfer.2007.11.063. Apr.
[39] Y. Li, J. Zhou, S. Tung, E. Schneider, S. Xi, A review on the development of nanofluid preparation and characterization, Powder. Technol. 196 (2) (2009) 89–101, https://doi.org/10.1016/J.POWTEC.2009.07.025. Dec.
[40] S. Suseel Jai Krishnan, M. Momin, C. Nwaokocha, M. Sharifpur, J.P. Meyer, An empirical study on the persuasive particle size effects over the multi-physical properties of monophase MWCNT-Al2O3 hybridized nanofluids, J. Mol. Liq. 361 (2022), https://doi.org/10.1016/j.molliq.2022.119668. Sep.
[41] A. Ahmadi Nadooshan, H. Eshgarf, M. Afrand, Measuring the viscosity of Fe3O4-MWCNTs/EG hybrid nanofluid for evaluation of thermal efficiency: newtonian and non-Newtonian behavior, J. Mol. Liq. 253 (2018) 169–177, https://doi.org/10.1016/J.MOLLIQ.2018.01.012. Mar.
[42] B. Choon Pak and Y.I. Cho, "Experimental heat transfer an international journal hydrodynamic and heat transfer study of dispersed fluids with submicron metallic oxide particles," 2007, 10.1080/08916159808946559.
[43] K.V. Sharma, L.S. Sundar, P.K. Sarma, Estimation of heat transfer coefficient and friction factor in the transition flow with low volume concentration of Al2O3 nanofluid flowing in a circular tube and with twisted tape insert, Int. Commun. Heat Mass Transf. 36 (5) (2009) 503–507, https://doi.org/10.1016/j.icheatmasstransfer.2009.02.011.
[44] C.O. Popiel, J. Wojtkowiak, Simple formulas for thermophysical properties of liquid water for heat transfer calculations (from 0°c to 150°c, Heat Transf. Eng. 19 (3) (1998) 87–101, https://doi.org/10.1080/01457639808939929.
[45] I.U. Ibrahim, M. Sharifpur, J.P. Meyer, Experimental investigations of particle sizes effects on exergy and entropy characteristics of AL2O3 - MWCNT hybrid nanofluid along the transitional flow regime, Case Stud. Therm. Eng. 51 (2023) 103575, https://doi.org/10.1016/J.CSITE.2023.103575. Nov.
[46] L.S. Sundar, M.K. Singh, A.C.M. Sousa, Enhanced heat transfer and friction factor of MWCNT-Fe3O4/water hybrid nanofluids, Int. Commun. Heat Mass Transf. 52 (2014) 73–83, https://doi.org/10.1016/j.icheatmasstransfer.2014.01.012. Mar.
[47] S.I. Abu-Eishah, Correlations for the thermal conductivity of metals as, Int. J. Thermophys. 22 (6) (2001) 1855–1868.
[48] J.P. Meyer, M. Everts, Single-phase mixed convection of developing and fully developed flow in smooth horizontal circular tubes in the laminar and transitional flow regimes, Int. J. Heat. Mass Transf. 117 (2018) 1251–1273, https://doi.org/10.1016/J.IJHEATMASSTRANSFER.2017.10.070. Feb.
[49] P. Dunn and M. Davis, *Measurement and data analysis for engineering and science*. 2017. Accessed: Oct. 07, 2023. [Online]. Available: https://books.google.com/books?hl=en&lr=&id=bmlQDwAAQBAJ&oi=fnd&pg=PP1&ots=H0LAUUIWz2&sig=Mi44eXrMD0KQ0w6qWH3ns-48R7o.
[50] A.J.G. Yunus, A. Cengal, Heat and mass transfer: fundamentals and applications, Heat Mass Transf. 1 (2014) 67–142, 379–424Accessed: Jun. 09, 2023. [Online]. Available: https://books.google.com/books/about/Heat_and_Mass_Transfer_Fundamentals_and.html?id=B89MnwEACAAJ.
[51] L.S. Sundar, K.V. Sharma, Heat transfer enhancements of low volume concentration Al2O3 nanofluid and with longitudinal strip inserts in a circular tube, Int. J. Heat Mass Transf. 53 (19–20) (2010) 4280–4286, https://doi.org/10.1016/j.ijheatmasstransfer.2010.05.056.
[52] S. Ponnada, T. Subrahmanyam, S.V. Naidu, A comparative study on the thermal performance of water in a circular tube with twisted tapes, perforated twisted tapes and perforated twisted tapes with alternate axis, Int. J. Therm. Sci. 136 (November 2018) (2019) 530–538, https://doi.org/10.1016/j.ijthermalsci.2018.11.008.
[53] C. Jumpholkul, et al., Experimental investigation of the heat transfer and pressure drop characteristics of SiO2/water nanofluids flowing through a circular tube equipped with free rotating swirl generators, Heat Mass Transf. und Stoffuebertragung 56 (5) (2020) 1613–1626, https://doi.org/10.1007/s00231-019-02782-z.
[54] A. Feizabadi, M. Khoshvaght-Aliabadi, A.B. Rahimi, Experimental evaluation of thermal performance and entropy generation inside a twisted U-tube equipped with twisted-tape inserts, Int. J. Therm. Sci. 145 (August) (2019) 106051, https://doi.org/10.1016/j.ijthermalsci.2019.106051.
[55] A.S. Dalkılıç, O.A. Türk, H. Mercan, S. Nakkaew, S. Wongwises, An experimental investigation on heat transfer characteristics of graphite-SiO2/water hybrid nanofluid flow in horizontal tube with various quad-channel twisted tape inserts, Int. Commun. Heat Mass Transf. 107 (June) (2019) 1–13, https://doi.org/10.1016/j.icheatmasstransfer.2019.05.013.
[56] D. Madhesh, R. Parameshwaran, S. Kalaiselvam, Experimental investigation on convective heat transfer and rheological characteristics of Cu-TiO2 hybrid nanofluids, Exp. Therm. Fluid Sci. 52 (2014) 104–115, https://doi.org/10.1016/j.expthermflusci.2013.08.026.
[57] C.J. Ho, Y.J. Lin, Turbulent forced convection effectiveness of alumina-water nanofluid in a circular tube with elevated inlet fluid temperatures: an experimental study, Int. Commun. Heat Mass Transf. 57 (2014) 247–253, https://doi.org/10.1016/j.icheatmasstransfer.2014.08.017.
[58] A.J. Ghajar and L.-M. Tam, "Heat transfer measurements and correlations in the transition region for a circular tube with three different inlet configurations," 1994.
[59] J.P. Meyer, J.A. Olivier, Transitional flow inside enhanced tubes for fully developed and developing flow with different types of inlet disturbances: part I - Adiabatic pressure drops, Int. J. Heat. Mass Transf. 54 (7–8) (2011) 1587–1597, https://doi.org/10.1016/j.ijheatmasstransfer.2010.11.027. Mar.
[60] J.P. Meyer, J.A. Olivier, Transitional flow inside enhanced tubes for fully developed and developing flow with different types of inlet disturbances: part II-heat transfer, Int. J. Heat. Mass Transf. 54 (7–8) (2011) 1598–1607, https://doi.org/10.1016/j.ijheatmasstransfer.2010.11.026. Mar.

[61] H.R. Nagendra, Interaction of free and forced convection in horizontal tubes in the transition regime, J. Fluid. Mech. 57 (2) (1973) 269–288, https://doi.org/10.1017/S0022112073001151.
[62] R.M. Manglik, A.E. Bergles, Heat transfer and pressure drop correlations for twisted-tape inserts in isothermal tubes: part II—transition and turbulent flows, J. Heat. Transfer. 115 (4) (1993) 890–896, https://doi.org/10.1115/1.2911384. Nov.
[63] J.G. Withers, Tube-side heat transfer and pressure drop for tubes having helical internal ridging with turbulent/transitional flow of single-phase fluid. Part 1. Single-helix ridging, Heat Transf. Eng. 2 (1) (1980) 48–58, https://doi.org/10.1080/01457638008962750. Jul.
[64] T.C. Carnavos, Heat transfer performance of internally finned tubes in turbulent flow, Heat Transf. Eng. 1 (4) (1980) 32–37, https://doi.org/10.1080/01457638008939566. Apr.
[65] N.T. Obot, E.B. Esen, T.J. Rabas, The role of transition in determining friction and heat transfer in smooth and rough passages, Int. J. Heat. Mass Transf. 33 (10) (1990) 2133–2143, https://doi.org/10.1016/0017-9310(90)90115-B. Oct.
[66] M. Everts, J.P. Meyer, Relationship between pressure drop and heat transfer of developing and fully developed flow in smooth horizontal circular tubes in the laminar, transitional, quasi-turbulent and turbulent flow regimes, Int. J. Heat. Mass Transf. 117 (2018) 1231–1250, https://doi.org/10.1016/j.ijheatmasstransfer.2017.10.072. Feb.
[67] S.E.B. Maïga, C.T. Nguyen, N. Galanis, G. Roy, T. Maré, M. Coqueux, Heat transfer enhancement in turbulent tube flow using Al2O 3 nanoparticle suspension, Int. J. Numer. Methods Heat. Fluid. Flow. 16 (3) (2006) 275–292, https://doi.org/10.1108/09615530610649717/FULL/PDF.
[68] E. Manay, Emre Mandev, and E. Mandev, "Experimental investigation of mixed convection heat transfer of nanofluids in a circular microchannel with different inclination angles," *J. Therm. Anal. Calorim.*, vol. 135, 10.1007/s10973-018-7463-9.
[69] B. Fani, M. Kalteh, and A. Abbassi, "Investigating the effect of Brownian motion and viscous dissipation on the nanofluid heat transfer in a trapezoidal microchannel heat sink," 2014, 10.1016/j.apt.2014.08.009.
[70] Z. Haddad, E. Abu-Nada, H.F. Oztop, A. Mataoui, Natural convection in nanofluids: are the thermophoresis and Brownian motion effects significant in nanofluid heat transfer enhancement, Int. J. Therm. Sci. 57 (2012) 152–162, https://doi.org/10.1016/J.IJTHERMALSCI.2012.01.016. Jul.
[71] M. Sheikholeslami, M. Gorji-Bandpy, D.D. Ganji, P. Rana, S. Soleimani, Magnetohydrodynamic free convection of Al2O3–water nanofluid considering Thermophoresis and Brownian motion effects, Comput. Fluids. 94 (2014) 147–160, https://doi.org/10.1016/J.COMPFLUID.2014.01.036. May.
[72] D.A. Nield, A.V. Kuznetsov, The effect of vertical throughflow on thermal instability in a porous medium layer saturated by a nanofluid, Transp. Porous Media 87 (3) (2011) 765–775, https://doi.org/10.1007/s11242-011-9717-x.
[73] B.C. Pak, Y.I. Cho, Hydrodynamic and heat transfer study of dispersed fluids with submicron metallic oxide particles, Exp. Heat Transf. 11 (2) (1998) 151–170, https://doi.org/10.1080/08916159808946559.
[74] W. Yu, D.M. France, D.S. Smith, D. Singh, E.V. Timofeeva, J.L. Routbort, Heat transfer to a silicon carbide/water nanofluid, Int. J. Heat. Mass Transf. 52 (2009) 3606–3612, https://doi.org/10.1016/j.ijheatmasstransfer.2009.02.036.
[75] A. Meriläinen, et al., Influence of particle size and shape on turbulent heat transfer characteristics and pressure losses in water-based nanofluids, Int. J. Heat. Mass Transf. 61 (1) (2013) 439–448, https://doi.org/10.1016/J.IJHEATMASSTRANSFER.2013.02.032. Jun.
[76] M. Goharkhah, M. Ashjaee, M. Shahabadi, Experimental investigation on convective heat transfer and hydrodynamic characteristics of magnetite nanofluid under the influence of an alternating magnetic field, Int. J. Therm. Sci. 99 (2016) 113–124, https://doi.org/10.1016/J.IJTHERMALSCI.2015.08.008. Jan.
[77] M. Mehrali, et al., Heat transfer and entropy generation analysis of hybrid graphene/Fe3O4 ferro-nanofluid flow under the influence of a magnetic field, Powder. Technol. 308 (2017), https://doi.org/10.1016/j.powtec.2016.12.024.